

# Active corrosion protection capacity of phosphate–permanganate conversion coatings doped with cerium

O. Girčienė\*,

L. Gudavičiūtė,

A. Selskis,

V. Jasulaitienė,

A. Martušienė,

R. Ramanauskas

*Institute of Chemistry,  
State Scientific Research Institute  
Centre for Physical  
Sciences and Technology,  
Goštauto St. 9,  
LT-01108 Vilnius, Lithuania*

The aim of the present study was to develop the deposition process of cerium compound doped phosphate–permanganate conversion coating on the carbon steel surface and to evaluate its protective and self-healing capacities. The SEM and XPS techniques were applied to characterize the structure and composition of the investigated coatings. Voltammetric measurements were carried out to determine the protective ability of the passive layer, while EIS studies yielded information on the self-healing properties of different protective systems affected by introduced artificial defects. The phosphate–permanganate conversion coating on carbon steel was chosen as the base for deposition of cerium films from the  $\text{Ce}(\text{NO}_3)_3$  solution without and with  $\text{SO}_4^{2-}$  ions. The presence of permanganate in the phosphating solution and incorporation of Ce into the phosphate–permanganate layer on the steel surface increase the protective ability of the conversion coating. It was stated that the low frequency impedance has the same value as before the scratch formation. This suggests that the presence of Ce in the phosphate–permanganate coating leads to high values of low frequency impedance due to the healing of defects. These coatings provide corrosion protection for carbon steel and can be candidates for development of environmentally friendly pretreatments.

**Keywords:** corrosion protection, phosphate–permanganate conversion coating, deposition

## INTRODUCTION

Carbon steel is extensively used in industrial fields, however, its susceptibility to corrosion in many environments limits its applications. For years, chromating has been applied to produce corrosion resistant conversion layers onto different substrates. Chromate conversion coatings have unrivalled self-healing abilities, which are believed to arise from the migration of a soluble Cr(VI) compound in the coating to a scratch or defect, where they are reduced to form a new protection layer [1, 2]. The environmental hazards of conventional chromium-based conversion coatings have led to a worldwide search for an alternative.

Recently, lots of chromate free conversion coatings called “environmentally friendly” have been developed, such as permanganate [3, 4], phosphate–permanganate [5–9], rare earth and other based materials [10–20]. Manganese has been chosen due to its chemical similarities to chromium (structural and electronic) [4]. It is stated that permanganate coatings provide a good alternative to chromate conversion coatings because

they provide good corrosion resistance on magnesium and its alloys [3, 5–7], and on aluminium alloys [4, 8]. The phosphate–permanganate coatings are comparable to chromate conversion coatings for the protection of magnesium alloys, but unlike chromate conversion coatings, phosphate–permanganate coatings do not show any ability to regenerate [7].

Rare-earth salts, especially cerium and lanthanum salts, are known to inhibit the corrosion processes on several substrates, such as steel [10, 11], galvanised steel [12–14], aluminium and its alloys [15, 16], and magnesium alloys [17, 18]. These earth metal ions are non-toxic and environmentally friendly. The conversion coatings are obtained by dipping the metallic substrate in a solution of rare-earth salt. This procedure allows producing a protective surface film, which provides corrosion protection of metallic substrates. In a series studies on the use of cerium ion in protective coatings, Hinton and Wilson reported that the cerium ion, which acts as an inhibitor in the solution, was as effective as the chromium ion [19]. The action of the cerium ion resembled that of the chromium ion, and  $\text{CeO}_2$  acted as a barrier film. When a defect was generated, a cerium ion in the film repaired it, due to dissolution from the film and oxidation on the defect [20]. At the same time lack of data

\* Corresponding author. E-mail: olgag@chi.lt

on the protective abilities of manganese and cerium based conversion coatings on a steel surface can be stated.

The aim of the present study was to develop the deposition process of cerium compound doped phosphate–permanganate conversion coating on a carbon steel surface and to evaluate its protective and self-healing capacities.

## EXPERIMENTAL

### Materials and sample preparation

Carbon steel specimens, 10 × 20 mm and 1 mm thick with an area of 4 cm<sup>2</sup> previously polished with emery paper up to grade 400, degreased with ethanol and rinsed with distilled water, were used as base metal electrodes. The chemical composition of carbon steel is listed in Table 1. The following samples for comparison of their corrosion behaviour were investigated: polished carbon steel (CS), carbon steel coated with amorphous Fe phosphate (FeP), carbon steel coated with Mn conversion film (MnO) and MnO coated with cerium conversion coatings (Ce1 and Ce2).

Table 1. The elemental composition of the surface of investigated samples

Sample	Elements, at.% (by EDS)					
	O	P	Mn	Fe	S	Ce
CS	7.7	0.09	0.33	91.96	–	–
FeP	19.02	0.89	0.3	79.31	–	–
MnO	33.7	2.6	1.9	63.4	–	–
MnOCe1	36.88	1.19	0.32	60.21	–	1.4
MnOCe2	38.72	1.15	0.29	57.74	0.9	1.2

The phosphating solution was used for the formation of an amorphous FeP coating: 0.15 M H<sub>3</sub>PO<sub>4</sub>, 0.003 M H<sub>2</sub>C<sub>2</sub>O<sub>4</sub>, pH = 4–5, 50 °C, 10 min.

Phosphate–permanganate conversion coatings (MnO) were obtained by immersion of CS into the solution containing: 0.01 M KMnO<sub>4</sub>, 0.15 M H<sub>3</sub>PO<sub>4</sub>, 0.003 M H<sub>2</sub>C<sub>2</sub>O<sub>4</sub>, pH = 4–5, 70 °C, for 30 min.

Ce1 and Ce2 conversion coatings were formed by simple immersion of the samples for 24 h at 25 °C into solutions containing 0.05 M Ce(NO<sub>3</sub>)<sub>3</sub> and 0.05 M Ce(NO<sub>3</sub>)<sub>3</sub> + 0.025 M Na<sub>2</sub>SO<sub>4</sub>, respectively.

### Electrochemical measurements

The corrosion behaviour of samples was investigated in an aerated stagnant 0.5 M NaCl solution. The electrolyte was prepared from analytical grade chemicals and deionized water.

All electrochemical measurements were performed at ambient temperature with an Autolab PGSTAT302 potentiostat using a standard three-electrode system with a Pt counter electrode and a saturated Ag/AgCl reference electrode. All potentials are reported versus the saturated Ag/AgCl reference electrode. The corrosion current densities ( $i_{\text{corr}}$ ) were determined from voltammetric measurements by Tafel line extrapolation. A specimen was polarized with the potential scan rate of

0.5 mV s<sup>-1</sup>, from the cathodic to anodic region.

The measurements of electrochemical impedance spectra (EIS) were performed at the open circuit potential with the FRA2 module applying a signal of 10 mV amplitude in the frequency range 20 kHz to 0.001 Hz. The data obtained were fitted and analysed using the EQUIVCRT program of Boukamp [21].

### Morphology and composition

A microstructure and elemental composition of specimens were studied by a scanning electron microscope (SEM). A Helios NanoLab 650 dual beam workstation (FEI) with an X-Max 20 mm<sup>2</sup> energy dispersive detector (energy resolution of 127 eV for Mn Ka, Oxford Instruments) was used for imaging and energy dispersive analysis. Element mapping analysis was performed on the mechanically polished and vacuum carbon coated cross-sections of samples. The element mappings were carried out under the following measurement conditions: accelerating voltage 8 kV, beam current 3.2 nA, mapping resolution 512 × 352 pixels. X-ray line Ka (Si) was used for the characterization of element distribution on the sample surface. The deposited film thickness analysis was performed on the produced and vacuum Pt coated cross-sections of samples by the focused ion beam (FIB) technique.

The X-ray photoelectron spectroscopy (XPS) studies were performed by a spectrometer ESCALAB using X-radiation of MgK<sub>α</sub> (1253.6 eV, pass energy of 20 eV). To obtain depth profiles, the samples were etched in the preparation chamber by ionised argon at a vacuum of 5 × 10<sup>-4</sup> Pa. An accelerating voltage of ca 1.0 kV and a beam current of 20 μA cm<sup>-2</sup> were used.

## RESULTS AND DISCUSSION

### Formation of conversion coatings

The phosphate coating on the carbon steel FeP was chosen as the base for an active corrosion protection film. It is expected that an appropriate addition of another agent to the phosphate treatment solution may result in the synergetic effect on the protective properties of the conversion film. Permanganate in the phosphate solution acts as a strong oxidizing agent, which accelerates the dissolution of metal. Consequently, the presence of this compound influences the growth and modifies the structure of the conversion coating.

The phosphate–permanganate coating was formed in the solution, which contains acid phosphates of potassium and permanganate ions. Manganese is especially interesting in the conversion coating schemes due to its soluble high oxidation state Mn<sup>7+</sup> and insoluble lower oxidation states Mn<sup>3+</sup> and Mn<sup>2+</sup> [7].

Figure 1, curve 1 shows an alteration of the CS electrode potential ( $E_{\text{Me}}$ ) during immersion in the 0.01 M KMnO<sub>4</sub> + 0.15 M H<sub>3</sub>PO<sub>4</sub> + 0.003 M H<sub>2</sub>C<sub>2</sub>O<sub>4</sub> solution. At the initial stage of the conversion coating deposition, dissolution of the CS occurs, which is accompanied by a decrease in the  $E_{\text{Me}}$  value. Further, as the conversion coating grows, the value of  $E_{\text{Me}}$  increases over

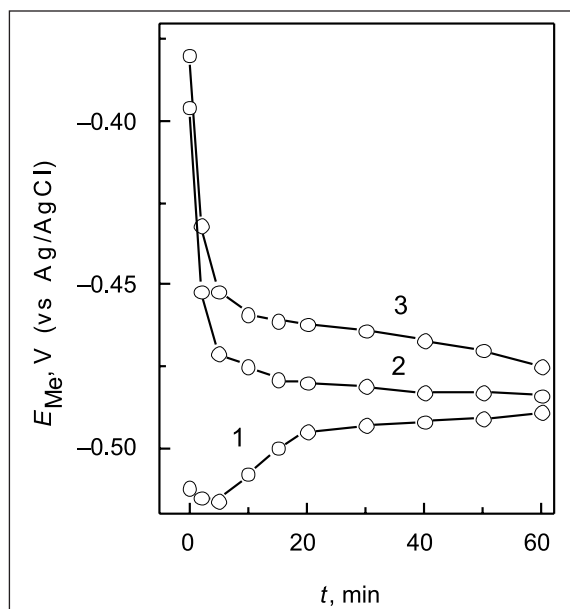
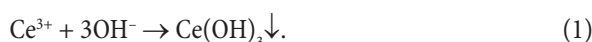


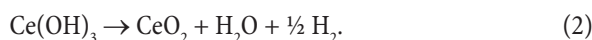
**Fig. 1.** Dependence of  $E_{Me}$  on time during the formation: (1) phosphate–permanganate MnO coating on CS in the 0.01 M  $KMnO_4$  + 0.15 M  $H_3PO_4$  + 0.003 M  $H_2C_2O_4$  solution, pH = 4, 60 °C; (2) Ce1 coating on MnO in the 0.05 M  $Ce(NO_3)_3$  solution, 25 °C; and (3) Ce2 coating on MnO in the 0.05 M  $Ce(NO_3)_3$  + 0.025 M  $Na_2SO_4$  solution, 25 °C

a period of 5–20 min. When the growth of film is completed,  $E_{Me}$  reaches a constant value. The observation implies that ca 20–30 minutes are enough to form a compact phosphate–permanganate layer on the steel surface.

The self-healing properties, which allow durable protection even after partial damage of the coating, can be achieved by introducing of specific corrosion inhibitors into the coating system. Ce ions were supposed to be such inhibitors, which can impart an active corrosion protection ability to the phosphate–permanganate conversion coating. When the metallic substrates are immersed into the conversion bath (pH ~ 5.5), the dissolution of the outer oxide layers is taking place [17]. This leads to the formation of cathodic activity and production of hydroxyl ions. Thus,  $Ce^{3+}$  precipitates as hydroxides:



With increase in the treatment time the cerium conversion film became richer in Ce(IV) species [17]. This evolution shows that either hydroxides are converted into oxides, or mainly oxides precipitate. The conversion of  $Ce(OH)_3$  into  $CeO_2$  has been mentioned in literature [22]. The presence of Ce(IV) could be due to the dismutation solid state reaction [17, 22]:



The alteration of the phosphate–permanganate deposit electrode in the  $Ce(NO_3)_3$  solution is presented in Fig. 1, curves 2 and 3. The deposition of cerium films on the investigated samples is accompanied by a decrease in the  $E_{Me}$  values

of the electrode, which reach some constant values after 40–60 min. However, more reproducible data were obtained when Ce based passivation continued for 24 h.

### Morphology and inner layer structure

An amorphous and compact phosphate layer of *c.a.* 200 nm thickness is deposited from the phosphating solution [23]. Meanwhile, the presence of permanganate in a phosphate solution influences the growth process and modifies the structure of the conversion coating. SEM images of the surface morphology and cross sections of the investigated phosphate–permanganate MnO coatings are presented in Fig. 2. The surface morphology of the coating (Fig. 2a) reflects the structure of the base steel surface, however, the thickness of the deposited layer is only *c.a.* 70–90 nm, which is significantly lower, with respect to the unmodified phosphate film [23], and may be related to the enhanced rate of the base metal dissolution. The colour of the phosphate–permanganate layer depends on the coatings thickness. The thinner coating was blue (70 nm), while the thicker one was yellow (90 nm). The phosphate–permanganate coatings are compact and possess good adherence to the base metal (Fig. 2b).

The SEM images of the morphology of both the Ce modified phosphate–permanganate coatings and the cross-sections of the same samples are presented in Fig. 3. The surface of

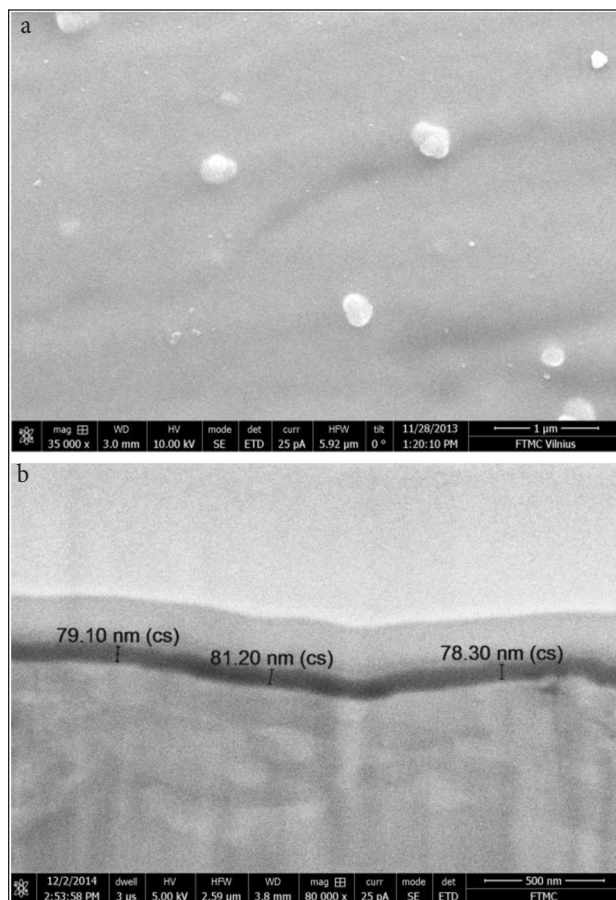


**Fig. 2.** SEM images of the microstructure (a) and cross-section (b) of MnO conversion coating on the carbon steel surface

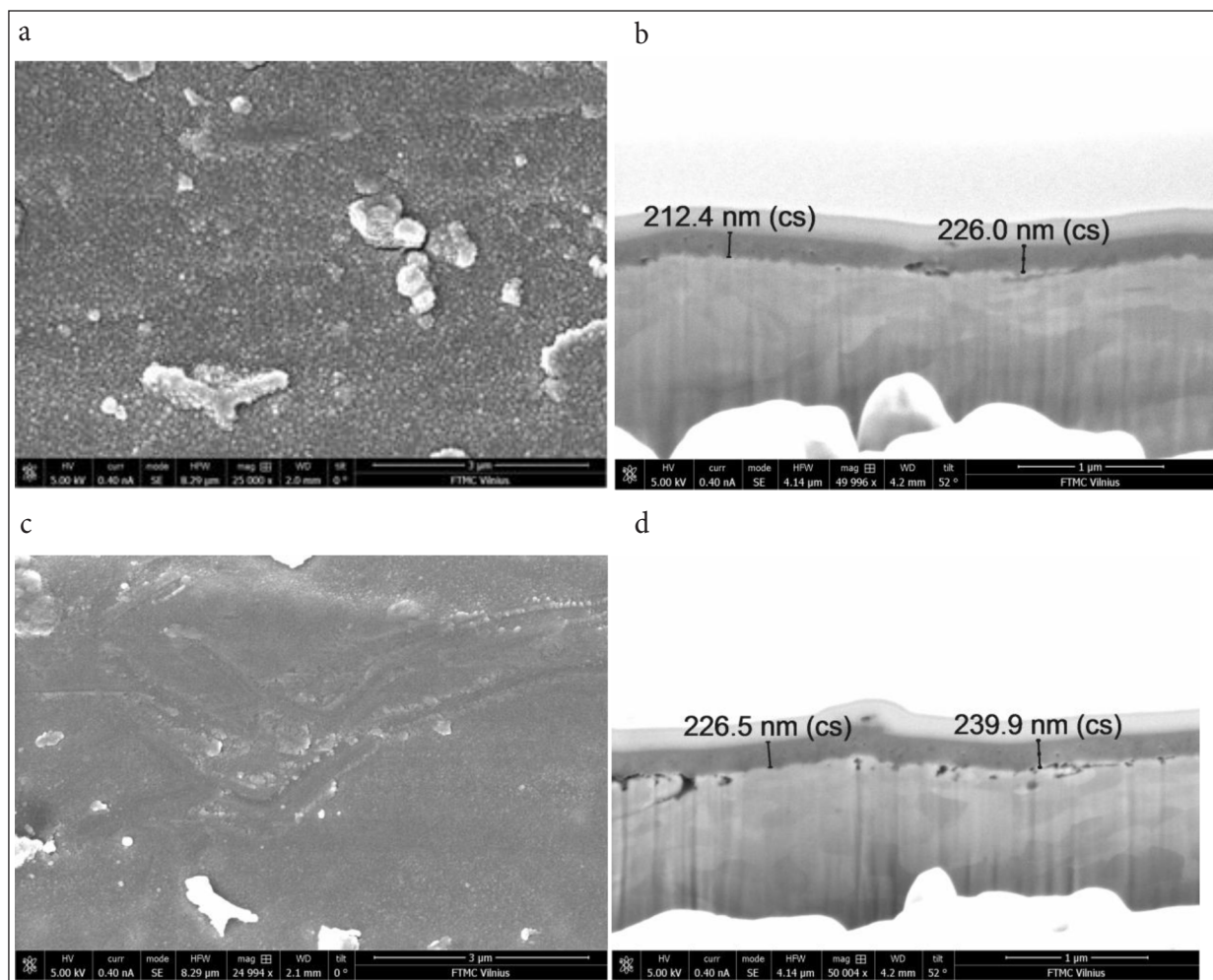


Fig. 3. SEM image of the microstructure (a, c) and cross-section (b, d) of MnOCe1 (a, b) and MnOCe2 (c, d) conversion coatings

MnOCe1 and MnOCe2 samples (Fig. 3a, c) reflects the morphology of the base surface with random crystalline aggregates, which are supposed to precipitate Ce oxide compounds according to Eqs. (1) and (2). The SEM images of cross-sections of these samples (Fig. 3b, d) indicate that the thickness of the coatings varied between 212–226 and 226–240 nm for MnOCe1 and MnOCe2 films, respectively. The presence of cavities in the boundary layer steel-conversion film was also characteristic of the Ce modified phosphate–permanganate coatings (Fig. 3b, d). The major thickness of the Ce modified phosphate–permanganate coatings is related to a significantly longer (up to 24 h) process duration, with respect to that of the unmodified coating, deposition of which lasted only 30 minutes. The presence of sulphate ions in the Ce deposition solution (MnOCe2 films) resulted in slightly thicker coating formation with respect to the coating deposited in the  $\text{Ce}(\text{NO}_3)_3$  unstirred solution (MnOCe1 film) (Fig. 3b).

## COMPOSITION

The analysis of elemental composition of the conversion coatings was performed by EDS and XPS measurements, the results

of which are listed in Tables 1 and 2. The EDS results indicate that all conversion layers were thin enough, as the most intensive signal (Fe) and the highest concentrations (58–79 at.%) were observed from the base metal. The next dominant element constituting the films is O (19–38 at.%), while the fact that the amount of P in a pure phosphate film, phosphate–permanganate and a Ce modified one varied between ~0.9 and 2.6 at.%. In addition, the phosphate–permanganate coatings contained up to 2 at.% of Mn, while the amount of this element in Ce modified coatings was lower and reached 0.3 at.%. The latter coatings possessed 1.2–1.4 at.% of Ce and the film formed in the solution containing sulfate ions (MnOCe2) additionally contained ~1 at.% of S. The results obtained imply that Fe oxides are one of the principal constituents of the formed conversion coatings.

The composition and the oxidation state of elements in the outer part of investigated conversion films were examined using XPS measurements. Mn  $2p_{3/2}$ , Ce 3d, O 1s, Fe  $2p_{3/2}$ , P 2p, N 1s, S 2p spectra were recorded after surface sputtering with  $\text{Ar}^+$  ions for an increasing period of time and the surface layer composition was determined and the results are listed in Table 2.

Table 2. XPS depth analysis of the investigated coatings

Sample	Depth,	Elements, at.%						
	nm	Ce	N	S	O	P	Fe	Mn
MnO	0	–	–	–	72.96	19	4.78	3.26
	5	–	1.64	–	61.91	17.83	15.66	1.79
	10	–	1.91	–	57.73	17.07	21.55	1.04
	20	–	1.28	–	59.99	14.59	22.35	1.22
MnOCe1 (Ce1-1h)	0	14.89	2.97	–	68.47	11.68	1.99	0.04
	5	18.13	1.73	–	57.12	14.38	7.99	0.66
	10	27.6	1.66	–	57.34	14.58	12.33	1.02
	20	7.8	1.39	–	58.55	14.47	16.66	1.13
MnOCe2 (Ce2-1h)	0	12.38	3.05	6.4	64.19	11.3	2.13	0.55
	5	24.82	1.22	1.82	55.12	12.84	4.18	0.09
	10	18.39	1.4	–	57.96	13.06	8.81	0.39
	20	10.4	1.35	3.8	58.36	13.79	15.6	0.5
MnOCe2 (Ce2-24 h)	0	21.31	1.12	7.3	61.92	6.04	2.07	0.38
	5	26.49	1.09	7.1	52.86	5.79	6.14	0.39
	10	27.11	0.61	3.99	53.72	9.08	5.48	0.42
	20	20.89	0.44	1.53	53.94	11.32	11.35	0.53

The Mn  $2p_{3/2}$  spectra of the phosphate–permanganate coating are presented in Fig. 4. It is evident that spectra are composed of an asymmetric peak. With an increase in sputtering depth, the intensity of the peak decreases, which implies the reduction of the Mn amount in deeper layers of the coating. The binding energy of this peak varied from 641.1 to 641.4 eV which suggests that Mn in the coating is of variable valence ( $Mn_3O_4$ , MnO,  $Mn_2O_3$ ) (Table 3). The Mn  $2p_{3/2}$  spectra of phosphate–permanganate samples doped with Ce1 and Ce2 show that the MnOCe1 coating was mainly composed of  $Mn_2O_3$ , MnO<sub>2</sub>, whereas MnOCe2, like an un-

modified phosphate–permanganate coating was composed of  $Mn_3O_4$ , MnO,  $Mn_2O_3$  (Table 3).

Table 3. XPS analysis data of Mn  $2p_{3/2}$  peak parameters for the investigated samples

Sputtering depth, nm	Binding energies, eV (Mn $2p_{3/2}$ )		
	MnO	MnOCe1	MnOCe2
0	641.10	–	–
5	641.37	642.81	642.91
10	641.42	643.25	640.80
20	641.22	642.51	641.20

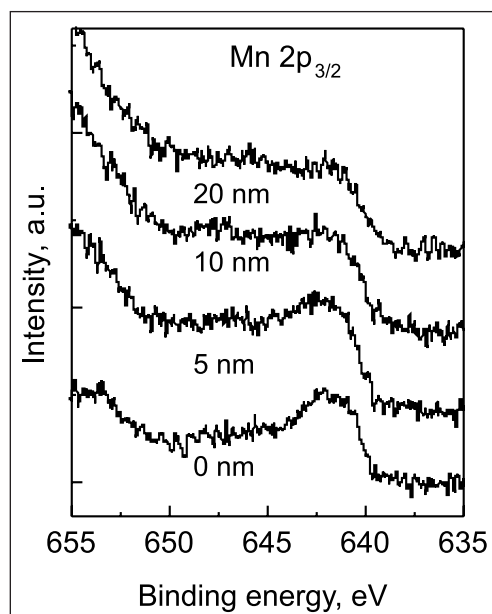


Fig. 4. XPS spectra for the Mn  $2p_{3/2}$  region obtained on the MnO coating

The quality of the Ce modified phosphate–permanganate films appeared to be significantly influenced by the process duration time. The Ce 3d spectra for MnOCe1 and MnOCe2 samples were identical, therefore, only the Ce 3d spectra of MnOCe2 coatings deposited during 1 and 24 h are presented in Fig. 5. In the Ce 3d spectra three different regions can be identified. The first one in the binding energy range from 880 to 890 eV corresponds to Ce  $3d_{5/2}$ , the second one for the binding energies from 890 to 910 eV includes the zone where the Ce  $3d_{3/2}$  and Ce  $3d_{5/2}$  spectra overlap, and the third one is due to the emergence of the satellite peak associated with Ce  $3d_{3/2}$  at a binding energy value close to 917 eV. This peak is of a crucial importance for determination of the oxidation state of cerium because its presence is only associated with Ce<sup>4+</sup> [12, 24]. Both samples MnOCe1 and MnOCe2 possessed the Ce  $3d_{3/2}$  peak at 916.3 eV characteristic of Ce<sup>4+</sup> [25], the intensity of which was not high and at a depth of 20 nm it was not observed even for the coatings deposited during 1 hour (Fig. 5a). When the deposition time of the Ce modified phosphate–permanganate coating was prolonged up to 24 hours, the intensity of the Ce<sup>4+</sup>

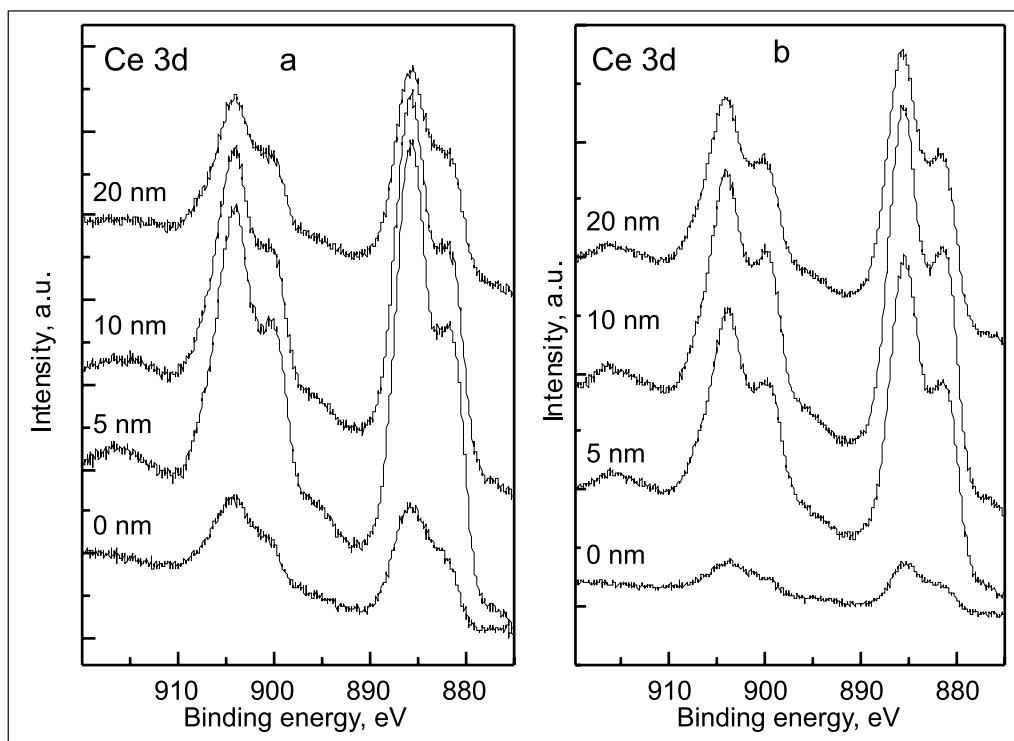


Fig. 5. XPS spectra for the Ce 3d region obtained on MnOCe2. Ce passivation time: (a) 1 h and (b) 24 h

peak increased (Fig. 5b). It is also evident that Ce like Mn compounds are located at the top layer of the conversion coating.

In general, according to the XPS measurements, in the top layer of the conversion coatings the highest concentrations of the constituent elements exhibited O, P, and Ce (Table 2). The effect of Ce modification duration influenced the P concentrations in the top layer, as it reduces P concentration two-fold in the samples modified for 24 h, with respect to that in the samples modified for one hour. Meanwhile, the amount of Mn depended neither on the modification time nor on the Ce solution composition. The overall concentrations of Ce in the modified coatings were close for the samples deposited from the solutions with and without sulphate ions. However, the higher amount of Ce, especially at a depth of 20 nm, was detected for the samples modified for 24 hours. It can be supposed therefore that during the extended modification of the phosphate–permanganate coating Ce compounds did not accumulate on the very top, but tend to penetrate into deeper layers of the coating.

Paying attention to the element, which may be responsible for the self-healing capability of conversion films, the oxidation states of Ce for different samples were evaluated. The percentage area of  $Ce^{4+}$  on the sample surface was calculated from the equation [16, 26, 27]:

$$Ce^{4+\%} = \mu\% / 14 \times 100, \quad (3)$$

where  $\mu$  is the satellite area percentage at 916.3 eV with respect to the total Ce 3d area. The percentage of  $Ce^{4+}$  to total Ce for

the MnOCe1 and MnOCe2 samples does not exceed 10%. This implies that phosphate–permanganate coatings contain Ce mainly in the form of  $Ce^{3+}$ . The presence of  $SO_4^{2-}$  ions in the Ce conversion film solution does not enhance the formation of Ce of a higher oxidation state.

### Protective ability

The corrosion behaviour of phosphate–permanganate coatings modified with Ce ions was investigated by the linear polarization and EIS measurements, which were carried out in a 0.5 M NaCl solution. The polarization curves of the investigated samples are shown in Fig. 6. The data obtained have shown that corrosion potential  $E_{corr}$  values of all samples with conversion coatings exhibited more positive  $E_{corr}$  as compared to those of CS and FeP (Table 4). The values of the  $i_{corr}$  were determined from the Tafel line extrapolation and the results obtained are listed in Table 5. The data obtained indicate that the presence of permanganate in the phosphating solution reduces the resulting coating thickness twofold, but at the same time decreases the corrosion current densities of the deposited samples from  $3.1 \cdot 10^{-6} \text{ A cm}^{-2}$  up to  $2.2 \cdot 10^{-6} \text{ A cm}^{-2}$ . As seen from the presented data, all samples coated with cerium exhibited the lowest values of  $i_{corr}$ , which varied in the range of  $0.7\text{--}1.1 \cdot 10^{-6} \text{ A cm}^{-2}$ . The protection efficiency  $P\%$  of samples was calculated by the equation [12, 13]:

$$P\% = (i_{corr}^0 - i_{corr}) / i_{corr}^0 \times 100, \quad (4)$$

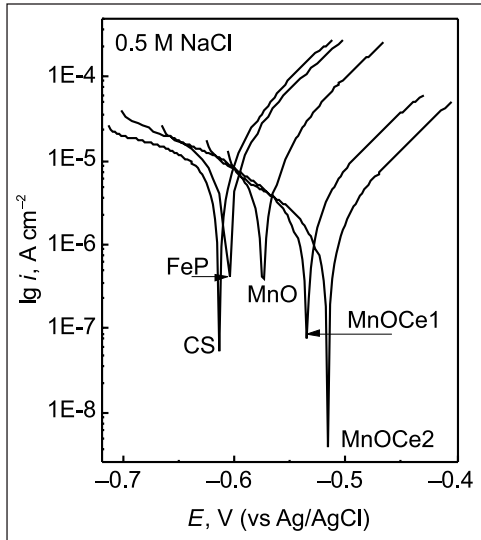


**Fig. 6.** Potentiodynamic polarization curves of the samples measured in 0.5 M NaCl solution at 25 °C, 0.5 mV s<sup>-1</sup>

where  $i_{\text{corr}}^0$  and  $i_{\text{corr}}$  denote the corrosion current density of bare steel and that of the electrode with the conversion coating, respectively. The calculated values of  $P\%$  increased from 41.5% for the FeP sample, up to ~79–88% for phosphate–permanganate samples coated with Ce1 or Ce2. The highest  $P\%$  value was stated for MnOCe2 (Table 4).

**Table 4.** The electrochemical parameters (corrosion potential  $E_{\text{corr}}$ , corrosion current density  $i_{\text{corr}}$ , polarization resistance  $R_p$ ) and protection efficiency ( $P\%$ ) of the investigated samples determined in 0.5 M NaCl solution

Sample	Electrochemical parameters				
	$E_{\text{corr}}$ V (vs Ag/AgCl)	$i_{\text{corr}}$ A cm <sup>-2</sup>	$P\%$ by Eq. (4)	$R_p$ kΩ cm <sup>2</sup>	$P\%$ by Eq. (5)
CS	-0.609	$5.3 \cdot 10^{-6}$	–	0.95	–
FeP	-0.588	$3.1 \cdot 10^{-6}$	41.5	1.65	42.4
MnO	-0.574	$2.2 \cdot 10^{-6}$	58.5	2.91	67.4
MnOCe1	-0.535	$1.1 \cdot 10^{-6}$	79.2	4.83	80.3
MnOCe2	-0.517	$6.5 \cdot 10^{-7}$	87.7	8.39	88.7

**Table 5.** EIS parameters obtained by fitting the Bode plots (Fig. 7) with the equivalent circuit  $R_1(Q_1[R_2(R_3Q_2)])$  measured in 0.5 M NaCl solution;  $R_1 = 2 \Omega \text{ cm}^2$

Sample	$R_2$ kΩ cm <sup>2</sup>	$Y_0(Q_1)/10^{-5}$ Ω <sup>-1</sup> cm <sup>-2</sup> s <sup>n</sup>	$n(Q_1)$	$R_3$ kΩ cm <sup>2</sup>	$Y_0(Q_2)/10^{-5}$ Ω <sup>-1</sup> cm <sup>-2</sup> s <sup>n</sup>	$n(Q_2)$
CS	–	–	–	0.95	89.3	0.82
FeP	0.004	7.3	1	1.64	77.6	0.61
MnO	0.02	13.2	0.63	2.89	42.5	0.62
MnOCe1	0.04	10	0.52	4.78	100.8	0.66
MnOCe2	0.15	25	0.5	8.24	38.2	0.62

EIS diagrams for the investigated samples exposed to the 0.5 M NaCl solution for 0.5 h are given in Fig. 7. The data

obtained were fitted and analysed using the EQUIVCRT program of Boukamp [21]. To interpret the EIS data, the  $R_1(Q_1[R_2(R_3Q_2)])$  equivalent circuit model, that is generally used to describe corrosion processes, was applied. The calculated parameters of the equivalent circuit were used for the simulation of impedance diagrams (Table 5). The polarization resistance  $R_p$  ( $R_p = R_1 + R_2 + R_3$ ) values of the investigated samples are listed in Table 4. An unmodified phosphate–permanganate sample possessed ~3 fold, whereas MnOCe1 and MnOCe2 from ~5 to 8 fold higher  $R_p$  values, respectively, as compared with those of CS.

The protection efficiency  $P\%$  of coatings was calculated using the following equation [28]:

$$P\% = (R_p - R_{p_{\text{pm}}}) / R_p \times 100, \quad (5)$$

where  $R_{p_{\text{pm}}}$  and  $R_p$  denote the polarization resistance of bare steel and that of the electrode with the conversion coating, respectively. The results obtained imply that the samples with the Ce2 conversion coating (MnOCe2) demonstrated better protective properties ( $P\% = 88.7\%$ ) in the 0.5 M NaCl solution (Table 4).

The MnOCe1 and MnOCe2 films were supposed to exhibit better protective abilities with respect to those of the CS, FeP and phosphate–permanganate samples. It can be stated, therefore, that the presence of permanganate in the phosphating solution and incorporation of Ce into the phosphate–permanganate layer on the steel surface increase the protective ability of the conversion coating.

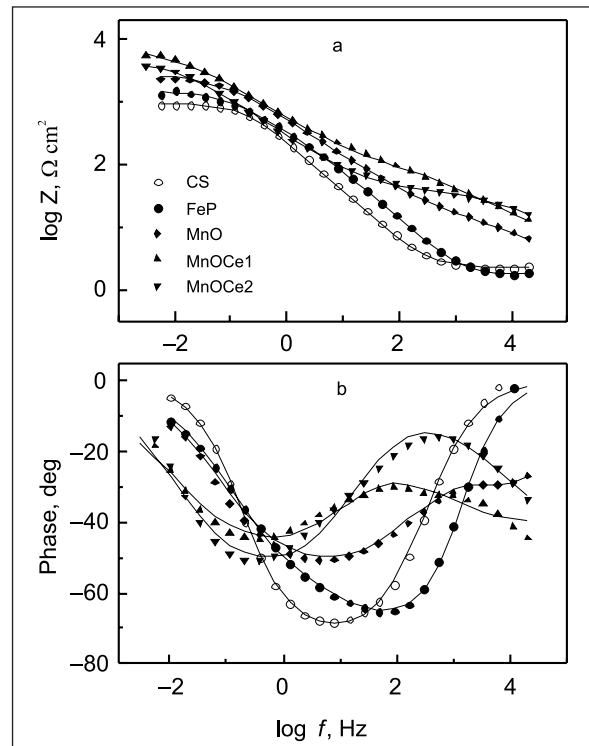


**Fig. 7.** Bode plots of EIS spectra after immersion of the samples in 0.5 M NaCl solution

### Self-healing ability

EIS technique can give important information on the kinetics of evolution of the coating degradation and the corrosion activity during immersion in the corrosive media. A high frequency part of the spectrum is usually related to the barrier properties of the coating, while a low frequency segment reflects the corrosion activity on the metal surface [29, 30].

An evolution of the impedance spectra for the phosphate–permanganate coating with defect formation after different periods of immersion in the 0.5 M NaCl solution is presented in Fig. 8. The artificial scratches were created by a sharp metallic needle. The Bode plot for the investigated sample before defect formation has two time constants. The resistive plateau at  $10^2$ – $10^4$  Hz represents the pore resistance of the coating, while the time constant at 0.01–1 Hz is related to the corrosion activity. The impedance values at 0.01–1 Hz after defect formation tend to continue the decrease for long immersion without any signs of recovery (Fig. 8). The decrease in impedance is caused by permanent development of corrosion processes in the defect zone.

The EIS spectra for the phosphate–permanganate coating modified with Ce ions (MnOce1 and MnOce2) during sample immersion in the 0.5 M NaCl solution before and after defect formation are given in Figs. 9 and 10, respectively. The Bode plot of the samples shows only two time constants without any signs of corrosion activity at low frequencies. Only the pore resistance of the coating decreases continuously. The low frequency impedance has the same value as before the scratch formation even after 2 hours of immersion in a chloride solution (Figs. 9 and 10). Thus, this suggests that the presence of Ce1 or Ce2 on the phosphate–permanganate coating can lead to high values of low frequency impedance due to the healing of the defect.

The results obtained imply that the modification of the phosphate–permanganate layer with Ce ions provides an active corrosion protection of the resulting conversion coating, however, regarding the low concentration of  $Ce^{4+}$  in the film and the presence of structural defects in the boundary base metal/coating, the self-healing capacities are not extremely high.

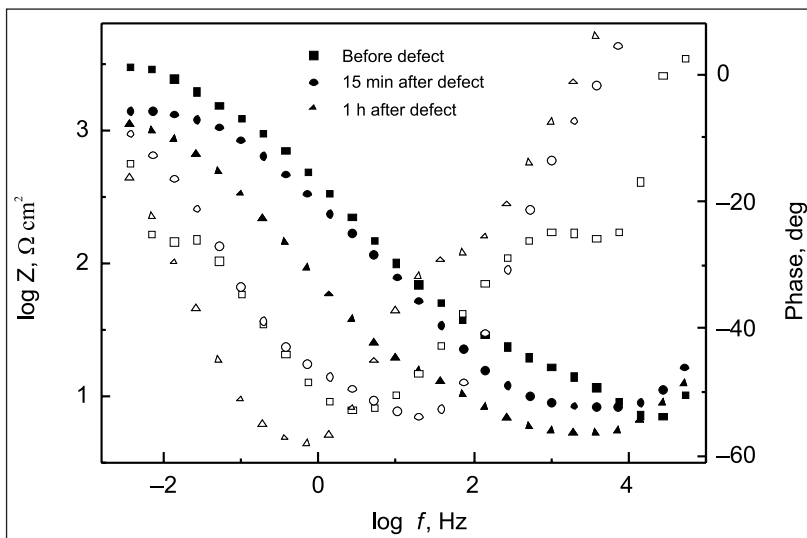


Fig. 8. Impedance spectra during MnO immersion in 0.5 M NaCl before and after defect formation

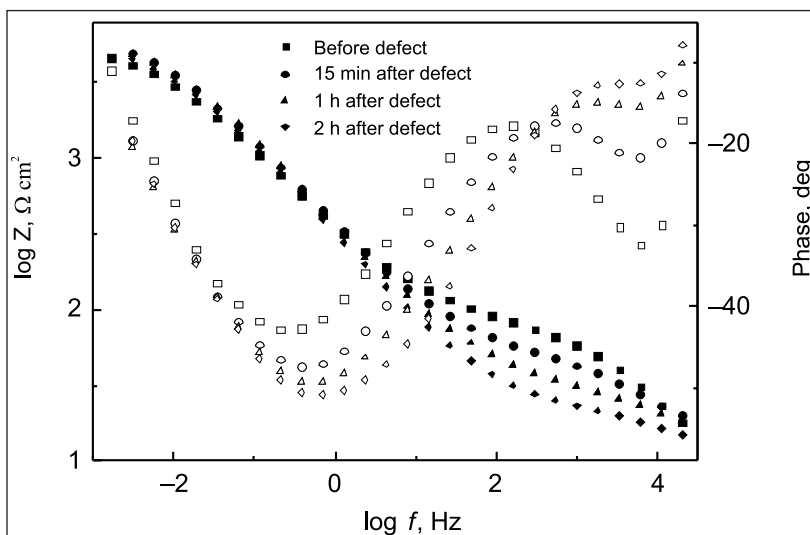
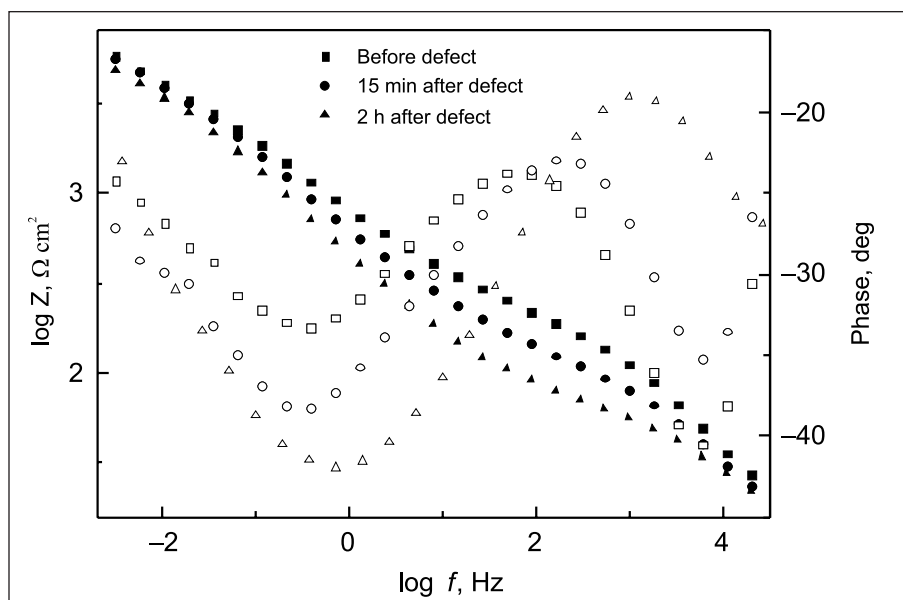


Fig. 9. Impedance spectra during MnOce1 immersion in 0.5 M NaCl before and after defect formation



**Fig. 10.** Impedance spectra during MnO/Ce<sub>2</sub> immersion in 0.5 M NaCl before and after defect formation

## CONCLUSIONS

A compact phosphate–permanganate conversion coating was deposited on the carbon steel surface from the permanganate containing a phosphoric acid solution. The presence of permanganate in the deposition solution reduces the thickness of the resulting coating twofold (up to 70 to 90 nm), but at the same time increases its protective ability. The thickness of the phosphate–permanganate coating modified with Ce varied between 212 and 240 nm and was slightly higher for the sample deposited from the sulphate containing solution.

EDS results imply that Fe oxides are one of the principal constituents of all deposited conversion coatings, while XPS data imply that Mn and Ce compounds are located in the top layer of the conversion film. The presence of Mn<sub>3</sub>O<sub>4</sub>, MnO, Mn<sub>2</sub>O<sub>3</sub> was identified in this layer, while in cerium–permanganate conversion coatings Ce is mainly present in the form of Ce<sup>3+</sup>.

The presence of permanganate in the phosphating solution and incorporation of Ce into the phosphate–permanganate layer on the steel surface increase the protective ability of the conversion coating.

EIS measurements were applied to study the self-healing processes in the conversion coatings. It was stated that the low frequency impedance has the same value as before the scratch formation. This suggests that the presence of Ce in the phosphate–permanganate coating leads to high values of low frequency impedance due to the healing of defects. Modification of the phosphate–permanganate layer with Ce ions provides an active corrosion protection of the resulting conversion coating, however, regarding the low concentration of Ce<sup>4+</sup> in the film and the presence of structural defects in the boundary base metal/coating, the self-healing capacities were not extremely high.

## ACKNOWLEDGEMENTS

This research was supported by the Research Council of Lithuania under Grant No. MIP – 029-2013.

Received 24 September 2015

Accepted 29 September 2015

## References

1. B. R. W. Hinton, *Met. Finish.*, **7**, 55 (1991).
2. J. E. Gray, B. Luan, *J. Alloys Compd.*, **336**, 88 (2002).
3. H. Umehara, M. Takaya, S. Terauchi, *Surf. Coat. Technol.*, **169–170**, 666 (2003).
4. I. Danilidis, J. Hunter, G. M. Scamans, J. M. Sykes, *Corros. Sci.*, **49**, 1559 (2007).
5. Y. L. Lee, Y. R. Chu, W. C. Li, C. S. Lin, *Corros. Sci.*, **70**, 74 (2013).
6. K. Z. Chong, T. S. Shih, *Mater. Chem. Phys.*, **80**, 191 (2003).
7. H. Zhang, G. Yao, S. Wang, Y. Liu, H. Luo, *Surf. Coat. Technol.*, **202**, 1825 (2008).
8. S. Pommiers, J. Frayret, A. Castetbon, M. Potin-Gautier, *Corros. Sci.*, **84**, 135 (2014).
9. A. J. Aldykewicz, H. S. Isaacs, A. J. Davenport, *J. Electrochem. Soc.*, **142**, 3342 (1995).
10. C. Wang, F. Jiang, F. Wang, *Corros. Sci.*, **46**, 75 (2004).
11. M. Fedel, A. Ahniyaz, L. G. Ecco, F. Deflorian, *Electrochim. Acta*, **131**, 71 (2014).
12. M. A. Arenas, J. J. de Damborenea, *Surf. Coat. Technol.*, **187**, 320 (2004).
13. Y. Kobayashi, Y. Fujiwara, *Electrochim. Acta*, **51**, 4236 (2006).
14. G. Bikulčius, A. Ručinskienė, A. Sudavičius, V. Burokas, A. Griguvevičienė, *Surf. Coat. Technol.*, **203**, 115 (2008).
15. X. Yu, G. Li, *J. Alloys Compd.*, **364**, 193 (2004).
16. S. Joshi, E. A. Kulp, W. G. Fahrenholtz, M. J. O'Keefe, *Corros. Sci.*, **60**, 290 (2012).
17. M. F. Montemor, A. M. Simões, M. J. Carmezim, *Appl. Surf. Sci.*, **253**, 6922 (2007).

18. M. F. Montemor, A. M. Simões, M. G. S. Ferreira, M. J. Carmezim, *Appl. Surf. Sci.*, **254**, 1806 (2008).
19. B. R. W. Hinton, L. Wilson, *Corros. Sci.*, **29**, 967 (1989).
20. R. G. Buchheit, S. B. Mamidipally, P. Schmutz, H. Guan, *Corros.*, **58**, 3 (2002).
21. B. A. Boukamp, *J. Electrochem. Soc.*, **142**, 1885 (1995).
22. A. J. Aldykewicz, A. J. Davenport, H. S. Isaacs, *J. Electrochem. Soc.*, **143**, 147 (1996).
23. O. Girčienė, R. Ramanauskas, V. Burokas, A. Martušienė, *Trans. Inst. Met. Fin.*, **82**, 137 (2004).
24. M. Hoang, A. E. Hughes, T. W. Turney, *Appl. Surf. Sci.*, **72**, 55 (1993).
25. G. Praline, B. E. Koel, R. L. Hance, H.-I. Lee, J. M. White, *J. Electron. Spectrosc. Relat. Phenom.*, **21**, 17 (1980).
26. J. Z. Shyu, K. Otto, W. L. H. Watkins, G. W. Graham, R. K. Beitz, H. S. Ghandi, *J. Catal.*, **114**, 23 (1988).
27. A. Pardo, M. C. Merino, R. Arrabal, F. Viejo, J. A. Muñoz, *Appl. Surf. Sci.*, **253**, 3334 (2007).
28. D. Weng, P. Jokiel, A. Uebleis, H. Boehni, *Surf. Coat. Technol.*, **88**, 147 (1996).
29. M. L. Zheludkevich, R. Serra, M. F. Montemor, K. Y. Yaskau, I. M. Miranda Salvado, M. G. S. Ferreira, *Electrochim. Acta*, **51**, 208 (2005).
30. M. L. Zheludkevich, K. A. Yasakau, A. C. Bastos, O. V. Karavai, M. G. S. Ferreira, *Electrochem. Commun.*, **9**, 2622 (2007).

**O. Girčienė, L. Gudavičiūtė, A. Selskis, V. Jasulaitienė, A. Martušienė, R. Ramanauskas**

### **FOSFATINIŲ-PERMANGANATINIŲ DANGŲ, PRATURTINTŲ CERIU, AKTYVIO APSAUGOS NUO KOROZIJOS GĖBA**

#### *S a n t r a u k a*

Darbo tikslas – paruošti fosfatinių–permanganatinių konversinių dangų, praturtintų cerio jonais, nusodinimo ant anglinio plieno technologiją ir ištirti jų apsaugines bei savaiminio užgijimo po įbrėžimo galimybes. Konversinių dangų struktūra bei sudėtis tirti SEM ir XPS metodais. Pasyvių sluoksnių apsauginės savybės nustatytos atliekant elektrocheminius tyrimus (voltamperometrija, EIS), savaiminis konversinių dangų užgijimas po įbrėžimo tirtas EIS metodu. Cerio plėvelės buvo nusodinamos ant fosfatinės–permanganatinės konversinės dangos iš  $\text{Ce}(\text{NO}_3)_3$  tirpalo be ir su  $\text{SO}_4^{2-}$  jonais. Fosfatinės–permanganatinės dangos praturtinimas Ce yra būtinas, kad šios dangos turėtų aktyvios apsaugos nuo korozijos gebą. Nustatyta, jog žemų dažnių impedanso vertės išlieka nepakitusios po tiriamosios dangos įbrėžimo. Esant Ce, dangose yra stebimos didelės žemo dažnio impedanso vertės, nulemtos defektuotų vietų savaiminio užgijimo. Šios dangos suteikia angliniam plienui korozinę apsaugą ir gali būti tyrimų objektu atliekant aplinkai draugiškų dangų paiešką.